Desalination and Water Treatment
www.deswater.com
doi: 10.5004/dwt.2020.25752

190 (2020) 279–293
June

Manganese removal and characterization of manganese oxides induced by biologically and chemically on the matured sand

Xiaoyu Wang, Yanling Yang, Xing Li, Zhiwei Zhou*, Xiaoyan Fan, Yuankun Liu, Nan Wang, Siyang Ji

College of Architecture and Civil engineering, Beijing University of Technology, No. 100 Xi Da Wang Road, Chao Yang District, Beijing 100124, P.R. China, Tel. +86 10 67391726; emails: hubeizhouzhiwei@163.com (Z. Zhou), 954787979@qq.com (X. Wang), yangyanling@bjut.edu.cn (Y. Yang), lixing@bjut.edu.cn (X. Li), 08254@bjut.edu.cn (X. Fan), liuyuankun@bjut.edu.cn (Y. Liu), 15011163966@163.com (N. Wang), 489506654@qq.com (S. Ji)

Received 18 September 2019; Accepted 14 February 2020

ABSTRACT

Manganese pollution particularly in the form of dissolved Mn^{2+} is an important problem in groundwater treatment. The main approaches for Mn^{2+} removal from groundwater are chemical catalytic oxidation and biological oxidation. Their relative attribution to Mn^{2+} removal and relationship has not been clarified at the matured stage. An influent of water containing 2.0 and 4.0 mg/L Mn^{2+} was filtered through columns filled with manganese sand that had either been inoculated with a manganese-adapted microbial community or had been pre-oxidized with potassium permanganate. Either treatment resulted in good manganese removal capacities that maintained a final concentration in the effluent below 0.05 mg Mn^{2+}/L at two concentrations for a period of 130 d. Among the matured period, the direct contribution rate of biological manganese removal was less than 20%. During operation, biological induction and chemical induction were both responsible for the formation of hexagonal Birnessite-type manganese oxide, whose physical characteristics were characterized and determined. Biological oxidation and chemical catalytic oxidation in the maturation of filter media were interlinked through the formation of Birnessite-type manganese oxide. Manganese removal during maturation was mainly attributed to cyclic autocatalysis rather than biological factors.

Keywords: Matured manganese removal filter; Hexagonal birnessite; Autocatalysis; Biological oxidation; Chemical catalytic oxidation

1. Introduction

Groundwater is a common source for production of drinking water [1], but potential pollution of groundwater with metal ions can pose serious problems. In particular, manganese can be commonly present in the form of dissolved Mn^{2+} [2]. Although manganese is an essential trace element for living organisms, it is toxic at relatively high concentrations and should be removed from drinking water to avoid adverse effects to human health. Excessive manganese concentrations (>0.1 mg/L) may discolor the water and produce an unpleasant metallic taste [3]. Chronic exposure to toxic concentrations of Mn^{2+} (>0.4 mg/L) can cause damage to brain and nervous tissue, and has been implicated as a possible cause for Parkinson's disease [4]. In China, the maximum recommended level of Mn^{2+} in drinking water is 0.1 mg/L, whereas the United States Environmental Protection Agency recommends a concentration lower than 0.05 mg/L. Therefore, manganese

* Corresponding author.

removal from groundwater is an essential step for drinking water production.

In order to meet water quality requirements, various methods have been adopted to reduce the concentration of manganese in water [5]. According to the redox potential-pH diagram of manganese in aqueous solution, its oxidation requires a relatively high redox potential [6], which is higher than the redox potential of most groundwater sources, so the oxidation of manganese in natural state is difficult to achieve. Adsorption of manganese to natural adsorbents such as activated carbon [7] or zeolite [8], or precipitation in combination with membrane filtration [2] has been studied to remove manganese from polluted water. However, most of the technologies have disadvantages of high operating costs, inadequate adsorption capacity or difficulties in sorbent separation.

Bio-oxidation and chemical catalytic oxidation separately employed with submerged rapid filtration are currently the most widely used processes for manganese removal [9,10]. The theory of bio-oxidation focuses on the bio-induction mechanism of promoting manganese oxidation. It has been suggested that the main reason for the bio-oxidation of manganese to manganese oxide is the direct enzymatic oxidation promoted by microorganisms [11]. Others have carried out the isolation and purification of engineering bacteria and optimization of culture conditions in order to obtain more efficient manganese-oxidizing bacteria (MOB) with higher manganese removal efficiency [12,13]. Compared with biological oxidation, the theory of chemical catalytic oxidation emphasizes that the removal of Mn^{2+} depends on the manganese oxides formed on the surface of the filter media. In this procedure most manganese is removed in the form of Birnessite-type manganese oxide [14]. The chemical kinetics of this process have been investigated [3], and the role of pH [5] and dissolved oxygen [15] or the synergistic removal of manganese and other pollutants [16,17] have all been studied.

However, the relationship between chemical catalytic oxidation and bio-oxidation has not been studied in detail. Most studies towards biological oxidation concentrate on the isolation and use of pure bacterial cultures, ignoring the fact that mixed communities of bacterial species typically form naturally during actual operation of water treatment. Researches towards chemical catalytic oxidation emphasize own catalytic role and often ignore the fact that microorganisms inevitably are present and involved in the process of manganese removal. In addition, most of the previous studies focused on the effects of biological or chemical mediation during the start-up stage of manganese removal [15,18], but less attention was given for the matured phases of the process.

This study systematically describes the prolonged removal of manganese from water under two different operation modes that are run in parallel: bio-induction and oxidant-induction. Reaction performance, the structure and activity of the manganese oxides formed by both processes are characterized and compared. The direct contribution rate of microorganisms to manganese removal in mature filter column was clarified. Clarification of the relationship between catalytic oxidation and bio-oxidation leads to a better understanding of the mechanism of overall manganese removal. In addition, this paper provides guidance for an effective or rapid removal of manganese during practical operation.

2. Materials and methods

2.1. Simulated raw water containing manganese

Mn^{2+} presence in groundwater was simulated by adding $MnSO_4{\cdot}H_2O$ to tap water at two concentrations: 2.0 ± 0.2 mg/L and 4.0 ± 0.1 mg/L. The tap water was left over 24 h to ensure the complete decay of residual chlorine before entering the influent tank. Since the used tap water already contains trace elements needed for microbial growth, no further components were added. The pH of used water was controlled to be 6.8–7.0 by adding diluted H_2SO_4 ($V_{H_2SO_4}$:V_{H_2O} = 1: 3), turbidity < 1.0 NTU, and contained concentrations of 7.0–9.1 mg/L dissolved oxygen (DO), 0.01–0.03 mg/L total iron and 125–145 mg/L HCO_3^-. Without addition of $MnSO_4{\cdot}H_2O$, the water had a manganese concentration below 0.05 mg/L. The temperature of used water was at the temperature of 25.0°C ± 1.0°C.

2.2. Rapid Set-up and operation of the experimental design

The experiments were performed with two identical laboratory-scale filter columns made of plexiglas (diameter: 3.0 cm; height: 150 cm), that received different treatments. The columns were designated *R*1 and *R*2, respectively (Fig. 1). The columns were filled by 100 cm height of manganese sand (Guangxi, China; 0.6–1.2 mm particle size) after sterilization. There was no MOB or other bacteria by measuring the quantities of microorganisms on the sterilized sand by autoclave sterilization. The manganese sand was mainly composed of psilomelane which have no catalytic ability. The bottom of column was composed of 10 cm pebbles (2–4 mm in diameter) to form a supporting layer. Two sampling ports were present, one at 20 cm below the sand level and one at the bottom, 100 cm below the sand level, that were used to extract both effluent and sand samples. The filter columns were operated in a downward flow mode at a filtration rate of 2 m/h. An overflow port was present at 10 cm below the top of each column to collect backwashing water.

Backwashing was carried out every 5 d of continuous operation and each backwashing lasted for 3 min. Backwashing was performed at a water flow intensity of 15–20 L/(s m^2) with dechlorinated tap water, resulting in a filter bed expansion of approximately 20%. Backwashing water entered the filter column from the bottom and flowed out through the overflow port, meanwhile the peristaltic pump was closed. Backwashing valves were closed and bottom outlet valves were opened during normal operation. Backwashing water and running effluent were discharged into sewer through pipeline.

Before experiment, column *R*1 was inoculated with a microbial community specialized in Mn^{2+} removal. For this, 20 L of backwash wastewater was collected from an actual groundwater manganese removal plant (located in Harbin, China) that had been in operation for more than 10 y. The outlet at the bottom of the filter column was connected

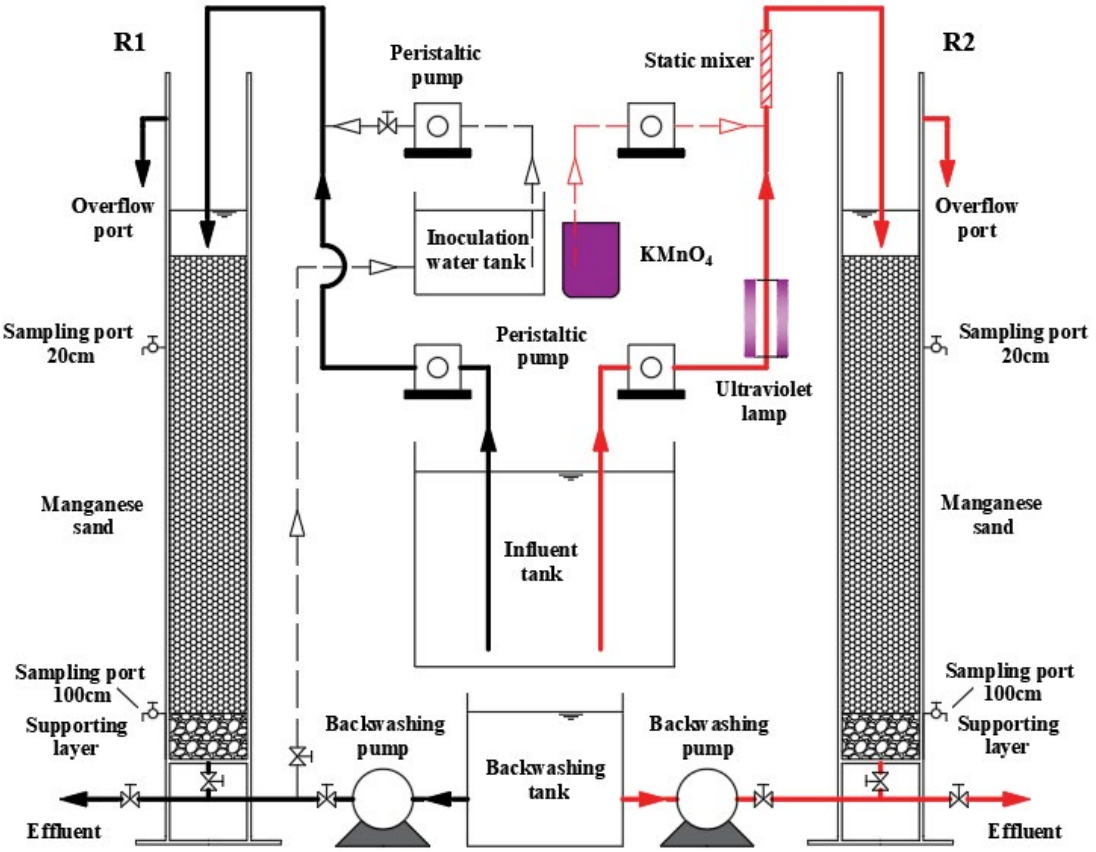

Fig. 1. Set-up of biologically and chemically induced manganese removal filters (thick solid lines represent the formal operation stage process, and thin dotted lines represent the chemically and biologically induced pre-treatments).

with the inoculation water tank through a pipeline, and the height of the inoculation water tank was adjusted to keep the water surface 10 cm above the sand surface of the filter column. The Mn^{2+} concentration of backwash wastewater was adapted to 2.0 mg/L by addition of $MnSO_4{\cdot}H_2O$, and then the backwash wastewater was circulated by peristaltic pump between *R*1 column (the thick dotted line of the *R*1 column in Fig. 1) and the inoculation water tank for 48 h at a filtration rate of 2 m/h, and followed by 24 h of soaking. Such inoculation process was repeated three times.

For *R*2 column, influent water passed through the irradiation of ultraviolet (UV) lamp (6 w, 0.44 mJ/cm^2) and then entered the column. The manganese sand in the *R*2 column was activated by pre-oxidation of Mn^{2+} in presence of potassium permanganate ($KMnO_4$) as Eq. (1):

$$3Mn^{2+} + 2MnO_4^- + 2H_2O \rightarrow 5MnO_2 + 4H^+ \quad (1)$$

For this, a static mixer was installed in front of *R*2 column which mixed a solution of 2.0 mg/L Mn^{2+} with 1.33 mg/L MnO_4–. The formed colloid of manganese oxide was introduced into the *R*2 column to precipitate and adhere to the surface of the sand (the thick dotted line of the *R*2 column in Fig. 1).

After 9 d induced initiation, the both columns of *R*1 and *R*2 were operated for a period of 100 d for removal of manganese from simulated raw water containing 2.0 mg/L Mn^{2+}, after which the concentration was increased to 4.0 mg/L Mn^{2+} for 30 d.

2.3. Batch experiment of matured manganese sand for manganese removal

The matured manganese sand was collected at 100 d of operation at 20 cm sampling port and separated into two parts, and filtered by a suction device to remove excess water. One part was sterilized in the 1% hydrogen peroxide (H_2O_2, 30% wt.%) and irradiated with UV lamps for 12 h. The UV lamps were opened turned on 30 min before the experiment to determine the constant UV intensity output. And the other part was directly used, so that the effect of biological activity could be separated from abiotic Mn removal. For each group of experiments, samples were taken to determine the quantities of bacteria to ensure that microorganisms were excluded. Ten aliquots of 0.5 g sand were weighed into 250 mL conical flasks containing 200 mL manganese solution (2.0 mg/L Mn^{2+}, pH 6.8). The flasks were plugged and shaken at 150 rpm and 25°C for 24 h. During this incubation, water samples were taken every 2 h for the detection of Mn^{2+} concentration.

2.4. Characterization

The matured manganese sand in section 2.3 was characterized, and the adhered manganese oxide was removed by ultrasonic oscillation (ultrasonic power 500 W, operating frequency 40 kHz). Subsequently, the samples of manganese sand were freeze-dried for 24 h and stored in a desiccator before measurement. The amount of manganese oxide on the surface of manganese sand was determined by acid digestion [19].

Surface morphology of the sand before the start of the experiment and after termination of the treatment was investigated by a scanning electron microscopy (SEM) (FEI Novanano450, Holland) operated at 10.0 kV. The composition elements of the manganese oxides were analyzed by using energy-dispersive X-ray spectroscopy (EDS).

The powder X-ray diffraction (XRD) patterns of the samples were recorded using a Bruker-D8 Advance diffractometer with Cu-Kα X-ray radiation. The samples of manganese sand were analyzed in the 2θ range of 5°–100° at a scanning speed of 5°/min.

Raman spectroscopy was performed with microscope Raman spectrometers (JY HR-800, Horiba) under the conditions previously described [14], in order to avoid possible damage to the structure of samples from exposure to high power laser radiation (5 mA) for >120 s.

X-ray photoelectron spectroscopy (XPS) was recorded by means of a K-Alpha X-ray photoelectron spectrometer (ESCALAB 250Xi, Thermo). The spectra were adjusted with respect to the *C*1s line of adventitious carbon at 284.8 eV.

2.5. Microbial analysis

For microbial analysis, the collected of manganese sand samples were used for bacterial DNA extraction using a DNA stool Mini Kit (Omega Bio-tek) following the manufacturer's protocol. The *V*3 region of the bacterial 16S rRNA gene was amplified by PCR using the primers 341F (5′-CCTACGGGAGGCAGCAG-3′) and 534R (5′-ATTACCGCGGCTGCTGG-3′) [13]. The PCR amplification started with initial denaturation at 95°C for 5 min, followed by 27 cycles of 95°C for 30 s, annealing at 55°C for 30 s and extension at 72°C for 45 s, with a final elongation at 72°C for 10 min. High-throughput sequencing was conducted with Illumina PE300 by BIOZERON Biotechnology Co. Ltd. (Shanghai, China). Reads were clustered into operational taxonomic units (OTUs) at 97% similarity. Bacterial community diversity was assessed by Shannon index, using the UPARSE pipeline.

2.6. Other analytic methods

The water samples need to be filtered through 0.45 μm membrane before detection. Total iron and total manganese concentrations were determined by the photometric method (the detection limit is 0.02 mg/L) according to standard methods for water and wastewater examination [20], using a multi-parameter spectrophotometer (LH-3BA, Lianhua Co., China). Temperature, pH and DO of the influent and effluent were measured by an online pH redox analyzer (MIK-PH4.0, MEACON Co., China) and a portable multi-parameter analyzer (HQ30d, HACH), respectively.

Filter media was collected every 10 d from the 20 cm outlet, the quantities of MOB being present were monitored by culture as described below: 1 mL filter media was diluted to 50 mL with sterile phosphate buffered solution and treated at 200 rpm by constant temperature oscillation incubator for 6 h to release attached bacteria. Bacteria were then serially diluted and cultured in the PYCM culture medium [12].

3. Results and discussion

3.1. Efficiency of manganese removal during long-term operation

At the beginning of the experiment, column *R*1 was inoculated with microorganism that was naturally present in wastewater of a groundwater manganese removal plant. After start-up period, the column was operated for removal of manganese from simulated raw water containing 2.0 mg/L Mn^{2+} for a period of 100 d, after which the concentration was increased to 4.0 mg/L Mn^{2+} for the last 30 d. Column *R*2, which was pre-loaded with manganese oxides in the 9 d start-up period, was run in parallel during the complete experiment. Effluent was tapped from two outlets positioned at a height of 20 from the top and at 100 cm located at the bottom of the column, respectively. Water samples were taken daily to monitor the manganese removal efficiency. Fig. 2 shows their respective manganese removal efficiencies and the quantities of MOB.

In the long-term operation of the manganese removal, the process can be divided into three stages. In the first stage, the removal of manganese mainly depended on the physical adsorption capacity of the filter media. With the gradual saturation of the adsorption capacity, the removal efficiency of manganese had been declining, even manganese leached from the filter column. The leaching of manganese occurred on the 11th day in the *R*1 column and on the 15th day in the *R*2 column, which was much lower than that of natural culture without intervention [20]. In addition, the concentration of manganese at 20 cm of *R*1 column was significantly higher than that in *R*2 column. During this period, MOB in *R*1 column could not contribute much to the removal of manganese because of the quantities, while manganese oxides in *R*2 column which had almost no microorganisms, had played a role in the removal of manganese.

The concentration of manganese in effluent was still decreasing after the saturation of the filter media, which was gradually coated by black manganese oxides. The ripening period of the filter media would be completed by biological effect and the catalytic of chemical oxidation. Through the manganese concentration curve of effluent at 20 cm of filter column, the change of manganese concentration during the ripening period of *R*1 and *R*2 could be well observed. The manganese concentration of *R*1 column declined slowly at the day of 20th to 28th, and rapidly decreased from 1.264 mg/L (removal rate was 35.15%) to 0.036 mg/L (removal rate was 98.20%) in 29th–45th day with the quantities of MOB reached 10^4–10^5. However, the manganese concentration of *R*2 column decreased steadily from 0.991 mg/L (removal rate 49.64%) to 0.013 mg/L (removal rate 99.34%) in 22th–42th day. The rapid stage of *R*1 column coincided with the appearance of MOB approaching the maximum value, which reflected that effective bio-induced manganese

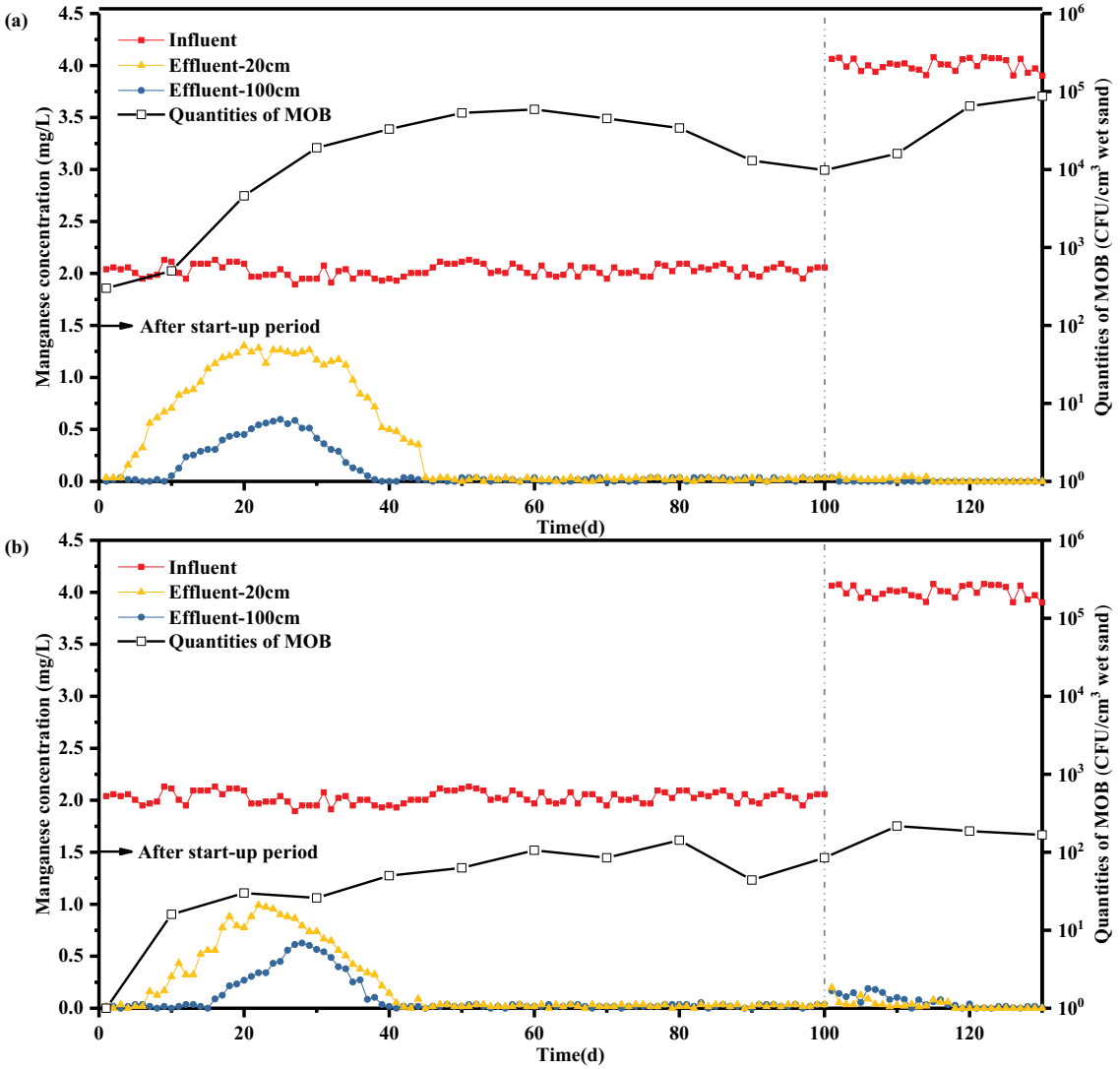

Fig. 2. (a) Manganese concentration (colored data points) and quantities of MOB (black data points) inside the columns during 130 d of operation for column *R*1 and (b) column *R*2. Note the difference in scale for MOB quantization between panels *A* and *B*.

removal required adequate amounts of MOB. However, the quantities of MOB in *R*2 column at this stage was less than 10^2 so that the microbial factors could be neglected, thereby the removal of manganese was mainly related to the manganese oxides formed during the start-up period. Although the sand had been sterilized, MOB and other microorganisms would still grow due to the impurity of backwash water and open environment of filter column. In the actual operation of the water plant, even though the effect of manganese removal by microorganisms was negligible, the impact of microorganisms on the device was inevitable. Interestingly, in the decreasing process of manganese concentration, the removal rate of *R*2 column depended on the part located within 20 cm, while the remaining part of *R*1 column still had strong removal effect on manganese. The reason for this phenomenon might be that manganese oxides mainly cover the upper end of *R*2 column in the start-up process, while MOB could distribute evenly throughout the filter column in the early stage.

The filter column could maintain the quality of the effluent for a long time after the maturation of filter media. From Fig. 2, it can be seen that the two filters exhibit similar capacity at this stage. The active parts of manganese removal were concentrated in the upper part of the filter column within 20 cm. When the manganese concentration was increased to 4 mg/L, the effluent of *R*2 column at 20 cm showed obvious fluctuation, which indicated that *R*1 column had better load shock resistance. The competition between manganese oxides and MOB existed in the matured filter column. The quantities of MOB decreased by an order of magnitude, while the removal efficiency of manganese did not decline. This part of manganese removal might be supported by manganese oxides. The concentration of manganese in effluent was below the detection limit for a long time when the filter media was matured. The contribution rate of manganese removal in this stage was discussed in the batch experiment.

The matured sand samples were incubated to determine their Mn removal efficiency in a batch experiment,

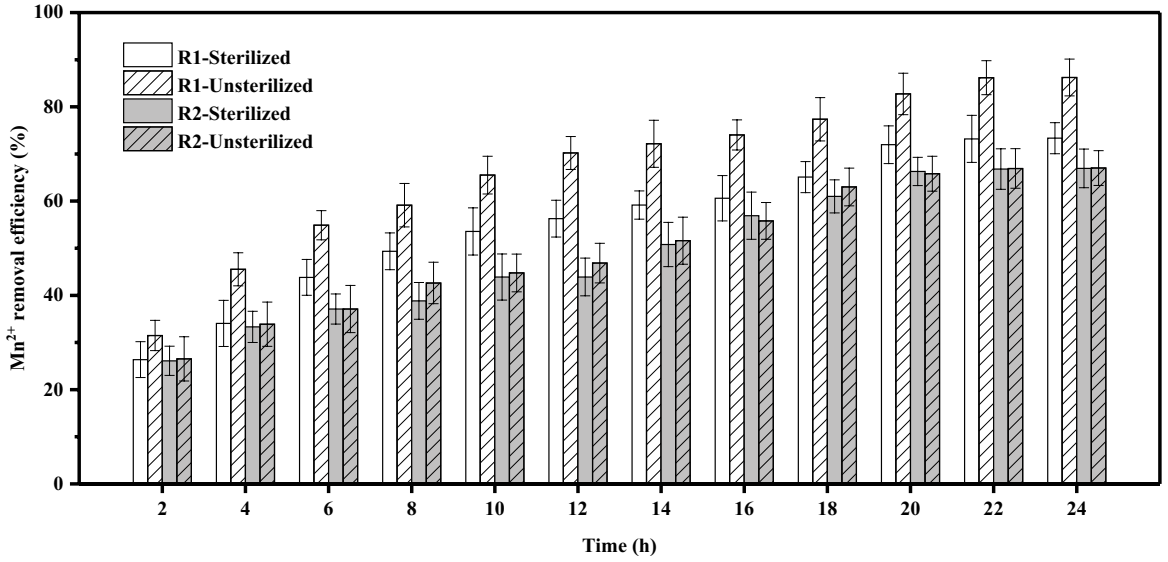

Fig. 3. Mn^{2+} removal efficiency between sterilized and unsterilized matured manganese sand of *R*1 and *R*2 column.=

whereby sterilized sand served as a control to clarify the effect of biological activity. The morphology of the manganese sand after sterilization was characterized by SEM (Fig. S1). Compared with the unsterilized sand, the damage on the physical structure of the manganese oxides film caused by sterilization was negligible. From the SEM images, oxide particles of different sizes were seen growing layer by layer with loose structure. The morphology of the manganese oxides film did not change obviously after sterilization, so the activity of manganese oxides did not damaged and the manganese oxide was not oxidized continuously by the sterilization, meaning the removal of Mn^{2+} was not affected by sterilization, which was consistent with previous studies [21,22]. As shown in Fig. 3, the Mn^{2+} removal efficiency of the matured manganese sands increased over time, for sand of *R*1 and *R*2, with or without sterilization. As expected, the removal efficiency of Mn^{2+} was highest with the unsterilized filter media of *R*1, compared with that of *R*2, indicating bio-induction had better manganese removal performance than the column *R*2 of chemical induction. The higher removal rate of unsterilized manganese sand of *R*1 than *R*2 might be due to the larger quantity of MOB and the difference of manganese oxides between them. When matured manganese sand of *R*1 was sterilized, the Mn^{2+} removal capacity decreased by almost 20%, indicating 80% of the removal was due to abiotic process. This revealed that there was limited direct bio-oxidation in the bio-inducted filter column, and most of manganese removal was completed by the manganese oxide formed by microorganisms. Thus, microorganisms would still generate and form manganese oxides to achieve manganese removal without induction by microbial or chemical oxidation, although this process might take more time. Interesting, the Mn^{2+} removal efficiency of *R*2 column with and without sterilization did not change significantly, confirming the biological oxidation had little effect on the removal of manganese. After sterilizing matured manganese sand of *R*1 and *R*2, the effect of microorganism was eliminated. At this time, it was confirmed that the number of manganese oxides on the surface of manganese sand or their structure and chemical composition were different, thereby resulting in the Mn^{2+} removal ability of *R*2 was still weaker than that of *R*1.

The amount of manganese oxide that had formed on the surface of the matured manganese sands was extracted by acid digestion and then quantified. The sand of the *R*1 column contained 0.146 g/g·sand, which was slightly higher than that of *R*2 (0.114 g/g·sand). The oxidation efficiency of manganese is directly related to the amount of manganese oxide being present [9,17]. That more manganese oxide is present in the sand of *R*1 explained its higher removal efficiency after sterilization compared to *R*2. In addition, the specific type and morphology of the manganese oxides that were deposited on the surface of filter media might also affect the removal efficiency [6,9].

The above results demonstrated that the biological oxidation and chemical catalytic oxidation both attributed to the Mn^{2+} removal, and manganese oxides acted more importantly.

3.2. Structure and characteristics of manganese oxide

The matured filter media from columns *R*1 and *R*2 was investigated by SEM imaging. Fig. 4a shows that virgin sand had a porous surface structure, which provided sufficient adsorption sites for attachment of bacteria, and contained a large effective surface area for physical adsorption of Mn^{2+} during the early stage of operation. After use in column *R*1, the sand was covered with microorganisms (Fig. 4b) (enlarged in the inset), which were mainly filamentous and rod-shaped bacteria. Microorganisms were co-localized with manganese oxides (Fig. 4b). An increased magnification of the deposited manganese oxide (insert Fig. 4c) revealed a porous sheet structure. After use in column *R*2, no bacteria were observed (Fig. 4d), as their numbers were much lower than in *R*1. The formed manganese oxides had a very different surface and appeared more sponge-like, with smaller

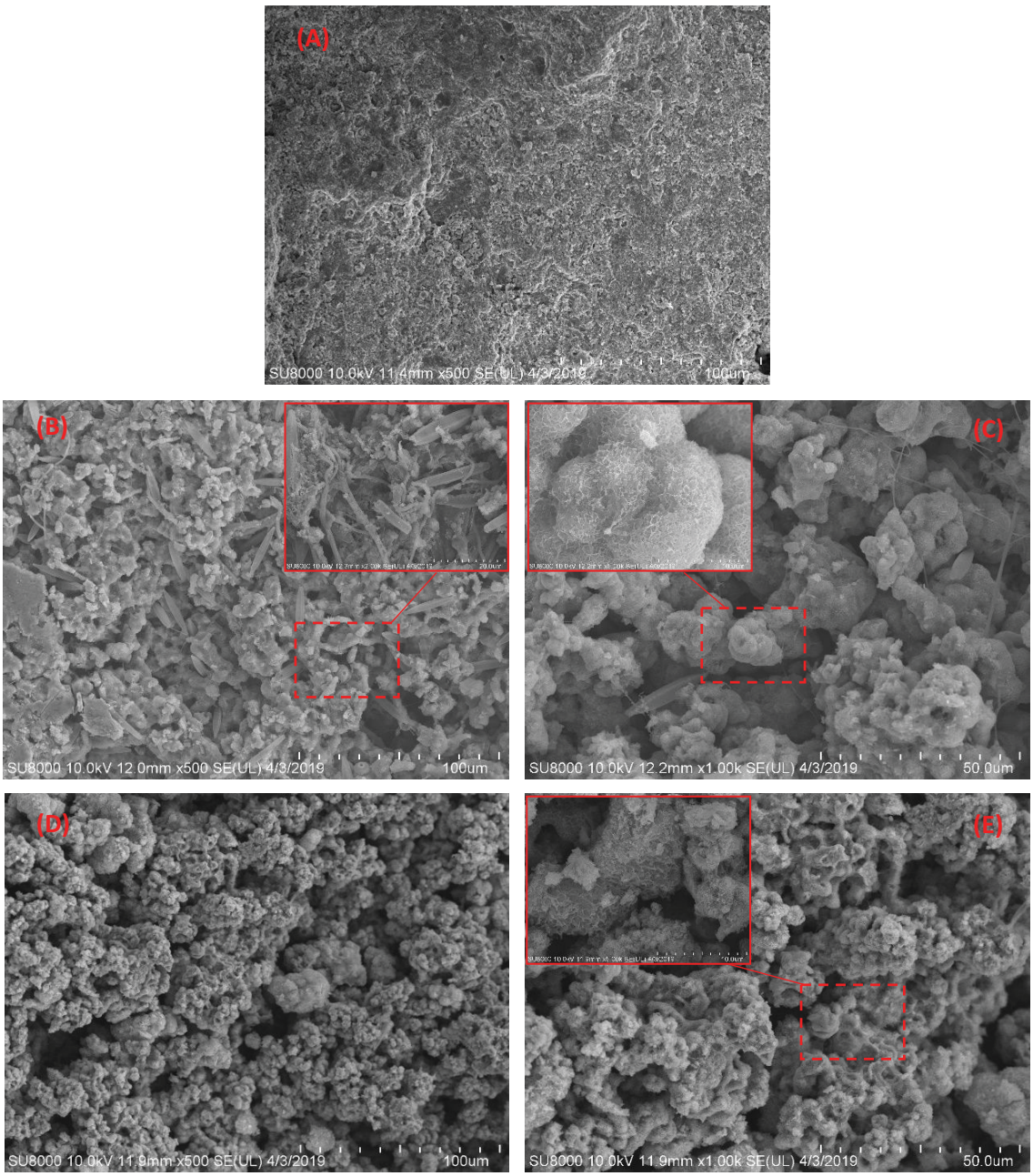

Fig. 4. (a) SEM image of manganese oxides on the surface of virgin sand, (b and c) and of sand collected after 100 d operation in column *R*1, (d and e) column *R*2. (b and d) the size bars indicate 100 μm (c and e) 50 μm in the main panels, while the inserts show increased magnification with a bar of 20 μm.

particle sizes and a compacter structure (Fig. 4e). This difference in morphology between biologically formed manganese oxides and chemically formed manganese oxides has been previously described [10,23]. The differences in surface structure and particle size of the manganese oxides deposited on sands of *R*1 and *R*2 was related to their different removal efficiency.

XRD analysis was performed to characterize the formed manganese oxides in more detail [24]. The obtained spectra produced overall low peak intensities (Fig. 5), with a number of broad peaks most likely originated from the manganese oxide. That these peaks were broad indicated a low crystallinity and a small crystal size of manganese oxides. Due to the poor crystallinity of the naturally formed Birnessite [25], it was difficult to completely match the obtained XRD peaks to that of artificial Birnessite. For comparison, the XRD pattern of triclinic Birnessite (JCPDS 43-1456) was inserted in the Fig. 5.

Four distinct peaks were identified, at 11.6°, 26.7°, 36.9°, and 66.0° (2θ) that are characteristic of Birnessite manganese oxide. The peak at 26.5° was the characteristic peak of SiO_2, which might be caused by the fall off of quartz sand in

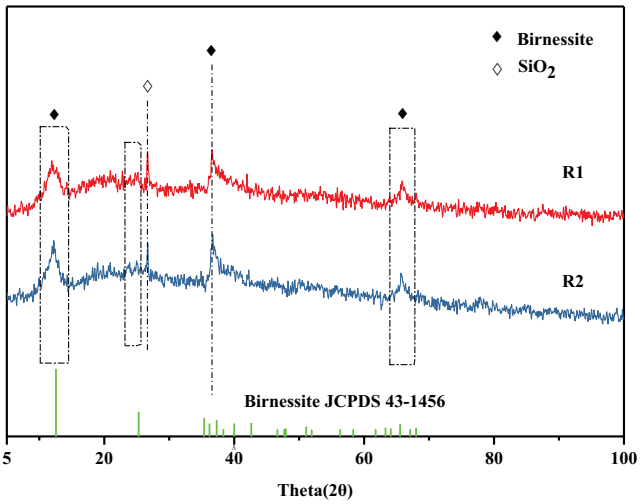

Fig. 5. XRD spectra of the manganese oxide deposited on the filter media of *R*1 (red spectrum) and *R*2 (blue spectrum). Typical peaks for crystalline Birnessite (JCPDS 43–1456, green) are indicated at the bottom. The regions of the spectra indicative of Birnessite are indicated by dotted squares and marked with a diamond.

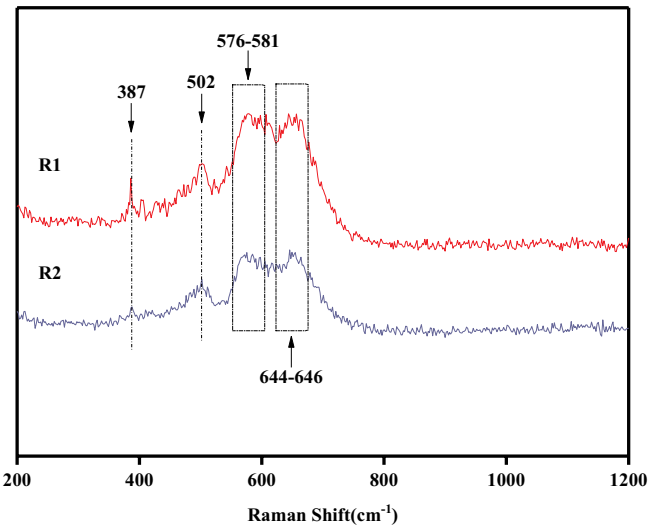

Fig. 6. Raman spectra of the manganese oxide deposited the filter media of *R*1 (red) and *R*2 (grey).

manganese sand. The peak values at 26.7° and 36.9° deviated from those of triclinic Birnessite (lower at 26.7° and higher at 36.9°), which were the obvious feature of the transformation from triclinic to hexagonal [26]. The XRD peaks at *d*-spacings of 7.3 Å (11.6° 2θ) assigned to a single hydration layer, respectively, which confirmed the intercalation of sodium (Na^+) in the Birnessite layer [27,28]. Moreover, the EDS images in Fig. S2 can also confirm the existence of Na^+ in manganese oxides. Peaks appearing at 11.6° and 26.7° (2θ) corresponded to 00L basal reflections. The observed low peak intensities and peak broadening of 00L revealed that stacking of the Birnessite sheets in both analyzed filter media was highly random [29]. The peaks at 36.9° and 66.0° (2θ) belonged to hk0 bands. Their asymmetry and wide peak width indicated a high turbostraticity and a hexagonal symmetry of the Birnessite [16]. It should be noted that the Birnessite-type manganese oxide formed during catalytic activity was composed of edge-shared MnO_6 [26]. Due to the high disorder of the MnO_6 layer and the large number of vacancies, the cations could be interlayer cation to form stable Birnessite. When the Birnessite was transformed from monoclinic, triclinic to hexagonal, cation exchange occurred between the hydration layers of Birnessite [28]. Besides, the presence of cations in the Birnessite layer could rapidly accumulate Mn(III) [30]. While the d-spacing of Mn^{2+} as interlayer cation of MnO_6 layer were the same as Na^+, resulting in the interlayer cations (such as Na^+) might be replaced by Mn^{2+}, especially in case of the single hydration layer structure of Birnessite [28].

XRD is not optimal for samples with poor crystallinity, for which Raman spectroscopy is more suitable. Fig. 6 shows the Raman spectra of the manganese oxide deposited on the two collected filter media. Three significant peaks appeared at 502, 576–581, and 644–646 cm^{-1}, three of all displayed the typical characteristics of Birnessite-type manganese oxide [30].

The Raman shift appearing at 644–646 cm^{-1} is considered to be produced by the Mn–O symmetric stretching vibration of the MnO_6 sheet plane, while the Raman shift at 576–581 cm^{-1} can be attributed to the Mn–O stretching vibration in the MnO_6 sheet plane [30]. In addition, the weaker Raman bands around 387 and 502 cm^{-1} are attributed to the bending vibration of Mn–O–Mn in hexagonal MnO_6 [31] The difference in peak heights between the two different samples was due to the different concentrations of metal counter-ions [30]. Different types of Birnessite-type manganese oxide were formed by interposition of different counter-ions between MnO_6 layers [31,32]. The Raman spectra confirmed that Birnessite-type manganese oxides were formed in both treatments, that had very similar structures, although the relatively weak spectra again indicated that the crystallinity of the Birnessite was poor or even amorphous, which was consistent with the results of XRD spectrum analysis.

Manganese oxides can exist in mixed valence states and this was analyzed by XPS analysis [33]. As shown in Fig. 7a, a Mn2p peak with value 642.2–642.3 eV appeared, which indicated that the average valence state of the manganese in the Birnessite was of a high valence state (+3 to +4), which explained why Birnessite had oxidation capacity. The XPS spectra were deconvoluted into different components to reveal the different valence states of the manganese oxides in the samples. The peak located at 640.2 eV was attributed to bivalent manganese (Mn(II), while peaks at 642.1 and 643.0 eV were attributed to Mn(III) and Mn(IV), respectively. After processing of the XPS data obtained with the sand from *R*1 and *R*2, similar atomic concentrations of Mn(II), Mn(III), and Mn(IV) were obtained (*R*1: 10.77%, 26.11%, and 63.12%; *R*2: 15.54%, 26.87%, and 58.59%), which indicated that the composition of the manganese oxide was similar in *R*1 and *R*2.

Manganese oxides coated media sample consisted of 100% Mn(IV) only possessed the adsorptive properties of general materials and need to be regenerated by oxidants such as potassium permanganate or chlorine [34]. However,

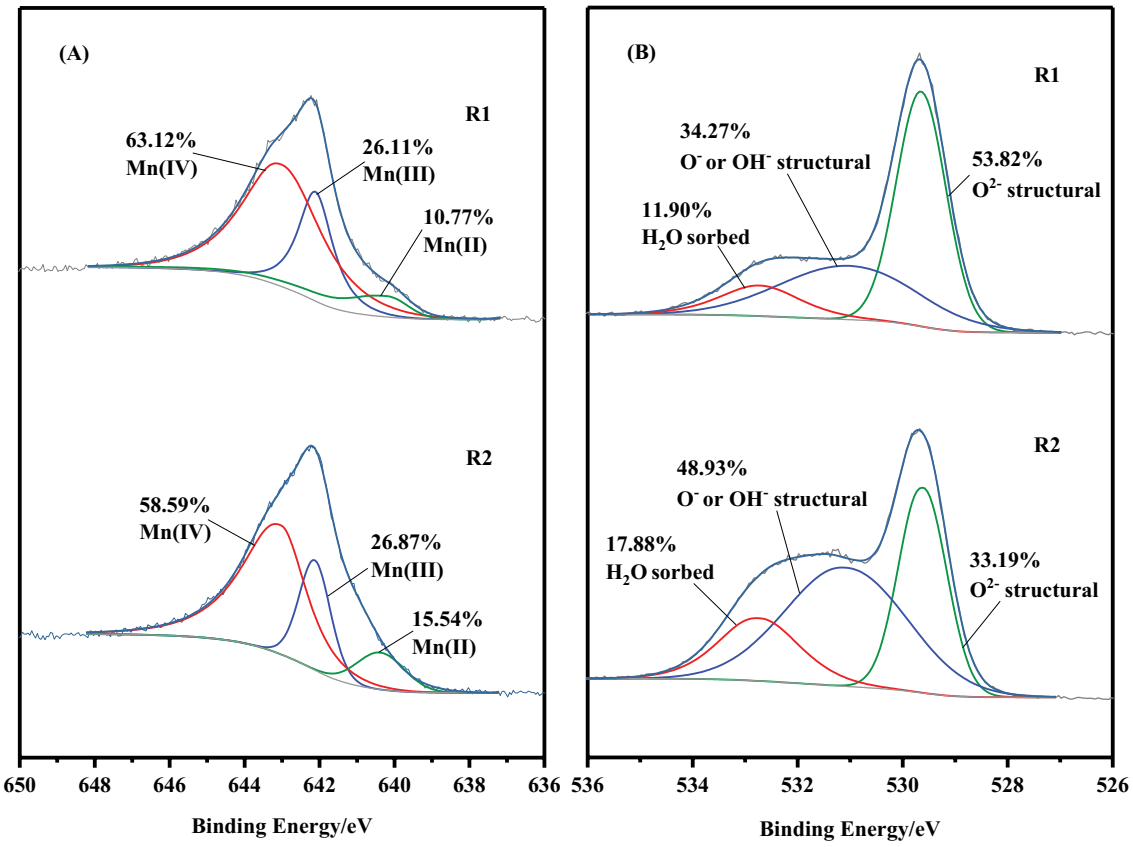

Fig. 7. XPS spectra of the (a) Mn2p and (b) O1s taken from manganese oxides that had formed during *R*1 and *R*2 treatment.

hexagonal Birnessite-type manganese oxide consists of Mn(II), Mn(III) and Mn(IV) [31], which can effectively guarantee the manganese removal process for a long time. Even though Mn(III) played an important role in the catalytic oxidation of manganese [23], the proposed cyclic auto-catalytic removal process of manganese could not be realized without the participation of Mn(II). The O1s spectra of the samples from *R*1 and *R*2 both reached a maximum at 529.6 eV, accompanied by a wide shoulder at higher binding energy. Three different types of surface oxygen were obtained from O1s spectra of the samples after peak-splitting fitting, as shown in Fig. 7b. The low peak at 529.6 eV was assigned to lattice oxygen (O^{2-}). The medium peaks at 531.0–531.3 eV corresponded to the adsorption of oxygen, such as structural O^- and OH^- groups. The high energy peaks located at 532.6–532.7 eV were assigned to surface adsorbed water [35,36]. The total concentration of adsorbed oxygen and lattice oxygen of *R*1 and *R*2 reached up to over 80%. Combined with the removal efficiency of manganese, it was concluded that the catalytic oxidation of manganese oxides was benefited from the substances formed by the bonds between manganese and oxygen. The surface adsorbed water was mainly responsible for chemical isomerization or structural binding [37], which was related to the hydration layer between MnO_6, but irrelevant with oxidation of manganese.

In conclusion, both bio-induction and chemical oxidant-induction produced hexagonal Birnessite. Among metal oxide catalysts, the way in which oxygen binds to metal was the most important for their catalytic performance. Bio-induction was more conducive to the formation of Mn(IV) and lattice oxygen, while chemical oxidant-induction resulted in formation of adsorbed oxygen. Compared with lattice oxygen, surface oxygen played a more critical role in the catalytic oxidation of Mn^{2+} [35]. This also explained the phenomenon shown in Fig. 3 that after the same treatment, the removal effect of *R*2 for Mn^{2+} was always less than that of *R*1. Moreover, Mn(II), Mn(III), and Mn(IV) were all involved in the catalytic oxidation for manganese removal.

A proposed reaction pathway is depicted in Fig. S3, showing a cyclic autocatalytic process for manganese removal. At the beginning of this process, metal cations (such as Na^+) in hexagonal Birnessite were easily replaced by Mn^{2+} (aq) in water. The Mn^{2+} (aq) absorbed onto the vacancy of MnO_6 sheets in hexagonal Birnessite where it formed Mn(II)–O, then reacted with Mn(IV) in the layer of MnO_6 to form Mn(III), subsequently, Mn(III) was oxidized to finally form a new hexagonal Birnessite. Based on this process, hexagonal Birnessite could achieve its own growth and result in continuous removal of manganese from the water.

3.3. Microbial community of manganese oxides on filter media surface

Although the above results confirmed that the manganese removal ability of matured filter media was not mainly due to biological effects, the direct contribution rate of

microorganisms in matured filter media was further studied. The microbial community that had built up in the matured manganese sand during treatment was characterized by high-throughput sequencing. The effective sequences generated could capture most of the bacteria based on good's coverage values (>99%) (Table S1). The Shannon's diversity index of *R*1 and *R*2 was 4.22 and 4.68, respectively (Table S1), suggesting the slightly higher bacterial diversity of *R*2 than *R*1. The competition of chemical catalysis for Mn^{2+} in *R*2 led to the lower Mn^{2+} concentration than that in R1 [38], which was one possible reason for the higher diversity of sample *R*2.

At phylum level, the dominant phyla (relative abundance >1% at least one sample) of *R*1 and *R*2 were investigated, and a total of seven dominant phyla were detected (Fig. 8a). Among them, *Proteobacteria* was the most abundant phylum in both samples, which accounted for 75.66% and 62.96% of the total sequences of *R*1 and *R*2, followed by *Actinobacteria*. Some members of *Proteobacteria* and *Actinobacteria* have been reported to have the capacities for biological manganese removal and the formation of Birnessite-type manganese oxides based on the culture-dependent methods [39]. *Proteobacteria* and *Actinobacteria* were also the dominant phyla in the manganese mineral containing Birnessite found in Danbong area, with relative abundance of 58% and 16%, respectively [38], which also indicated that the two phyla had relevance to Birnessite. Thus, the higher relative abundance of these two phyla in *R*1 (84.55%) than *R*2 (74.33%) was beneficial for achieving higher manganese removal efficiency in *R*1 (Fig. 8a). The relative abundance of *Proteobacteria* and *Actinobacteria* in *R*1 was higher than that of the inoculated water, which also indicated that the inoculation was successful and microorganism could adapt to the current water quality. The *Planctomycetes* and *Acidobacteria* were also the dominant phyla, and their relative abundances were comparable in *R*1 and *R*2. Moreover, it should be mentioned that *Candidatus Saccharibacteria* only occurred in *R*1 with relative abundance of 1.26%, while, *Acidobacteria* (4.56%) and *Verrucomicrobia* (5.56%) were the dominant phyla in *R*2, indicating the dissimilar bacterial community composition.

At genus level, there were 36.01% and 55.66% of the sequences in *R*1 and *R*2 were assigned as "unclassified genera", respectively, indicating that some new or unknown species were found in this study. The known genera with relative abundance above 1% were further screened (Fig. 8b), and 10 and 16 dominant genera were obtained in *R*1 and *R*2, respectively. The dominant bacteria in *R*1 were *Pseudomonas* (18.17%), *Pedomicrobium* (10.08%), *Nitrobacter* (6.07%), *Hyphomicrobium* (4.88%) and *Erythromicrobium* (4.17%). The dominant genera with relative abundance lowered than 4% were *Croceicoccus* (2.83%), *Gemmobacter* (2.45%), *Gp6* (1.47%), *Saccharibacteria_genera_incertae_sedis* (1.26%) and *Rhizorhabdus* (1.25%). For sample *R*2, Subdivision3_*genera_incertae_sedis* (3.84%), *Rubrivivax* (3.64%), *Reyrlla* (3.15%), *Nocardioides* (3.08%), *Pedomicrobium* (2.58%), *Hyphomicrobium* (2.36%), *Chryseolinea* (2.23%), and *Porphyrobacteria* (2.22%) were the dominant genera with relative abundance of 2%

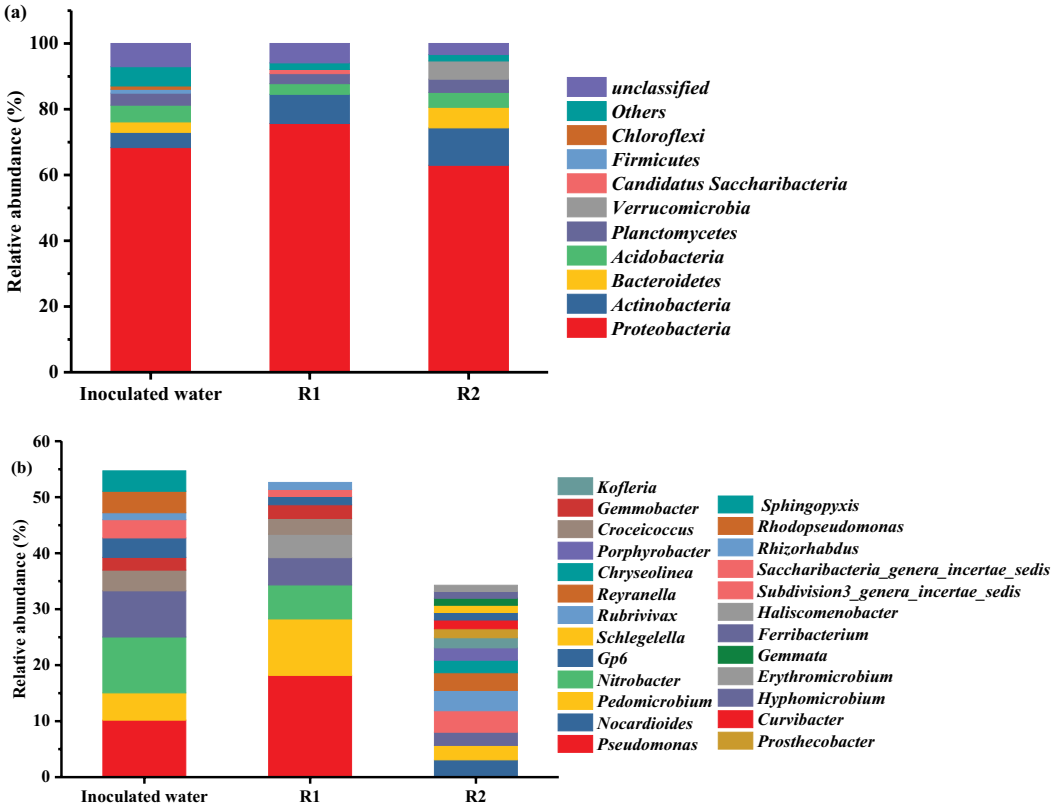

Fig. 8. Distributions of the bacterial community in inoculated water, *R*1 and *R*2: (a) at phylum level and (b) the dominant genera.

to 4%. Some other genera showed relative abundance lower than 2%, including *Kofleria* (1.79%), *Prosthecobacter* (1.62%), *Curvibacter* (1.56%), *Gp6* (1.33%), *Schlegelella* (1.3%), *Gemmata* (1.25%), *Ferribacterium* (1.21%) and *Haliscomenobacter* (1.12%). According to a summary of previous studies regarding MOB (Table 1), we found that *Pseudomonas*, *Pedomicrobium* and *Hyphomicrobium* were the effective MOBs for manganese removal in this study. The *Hypomicrobium* was an early discovered strain. In recent years, the research mainly focused on *Pseudomonas* and *Pedomicrobium*. The Mn^{2+} could be oxidized by the polymer production of *Pedomicrobium* [57]. While the oxidation of Mn^{2+} by *Pseudomonas* was dependent on the role of the Cu-dependent enzyme to form the Birnessite type manganese oxide [61]. Compared with the inoculated water, the relative abundance of *Pseudomonas*, *Pedomicrobium* in *R*1 increased, while the relative abundance of *Sphingopyxis*, *Rhodopseudomonas* decreased significantly. This phenomenon might be caused by the high manganese concentration and the lack of other nutrients. Moreover, the total relative abundance of the three genera in *R*1 was 6.71-fold higher than that of *R*2, which was consistent with the results of MOB quantities, further supporting the better higher manganese removal efficiency in *R*1. Moreover, although *Nitrobacter* is a common type of nitrite-oxidizing bacteria (NOB), which was also dominated in *R*1. A previous study has reported that MOB and NOB co-existed in the manganese removal system [1], which might assist MOB in manganese removal through electron transfer. Overall, *Pseudomonas*, *Pedomicrobium* and *Hyphomicrobium* were the dominant MOB and they were largely enriched in *R*1, enhanced the manganese removal efficiency and formed Birnessite-type manganese oxide.

Table 1
MOB reported in previous studies

Genus	References
Aerobacter	[40]
Arthrobacter	
Aurantimonas	[41]
Bacillus	[24,40,42–47]
Brevibacillus	[48]
Caulobacter	[40,49]
Chromobacterium	
Cytophaga	
Citrobacter	[40]
Corynebacterium	
Crenothrix	[50]
Erythrobacter	[41,51]
Gallionella	[40]
Hyphomicrobium	[40,49]
Janthinobacterium	[52]
Leptothrix	[40,52–56]
Lysinibacillus	[13]
Metallogenium	[50]
Pedomicrobium	[40,49,57]
Proteus	[40]
Pseudomonas	[40,49,58–60]
Siderocapsa	[12]
Siderocystis	
Streptomyces	[50]

4. Conclusions

The main conclusions of this work are as follow:

- Mn^{2+} was effectively removed using manganese sand as filter medium, either by bio-induction after inoculation with a suitable microbial community, or by chemical oxidation-induction by $KMnO_4$. Either treatment resulted in good manganese removal capacities that the leaching from column was shorten to around 25 d. Besides, the matured sand can maintain the continuous removal ability of manganese.
- The removal of Mn^{2+} was not significant until the quantities of MOB reached 104–105. The direct contribution rate of biological manganese removal was less than 20% on the matured sand, whereas that was mainly attributed to the cyclic autocatalytic process.
- Hexagonal Birnessite-type manganese oxides formed on the surface of matured manganese sands by either treatment. This immobilized Mn^{2+} by replacing interlayer cations and oxidized Mn(II) to Mn(III) under the action of Mn(IV), thus forming new Birnessite-type manganese oxides.

Acknowledgments

The authors acknowledge the financial support of the National Key Research and Development Program of China (2018YFC0406203 in 2018YFC0406200).

References

[1] F. Subari, M.A. Kamaruzzaman, S.R.S. Abdullah, H.A. Hasan, A.R. Othman, Simultaneous removal of ammonium and manganese in slow sand biofilter (SSB) by naturally grown bacteria from lake water and its diverse microbial community, J. Environ. Chem. Eng., 6 (2018) 6351–6358.
[2] S.F. Seyedpour, A. Rahimpour, H. Mohsenian, M.J. Taherzadeh, Low fouling ultrathin nanocomposite membranes for efficient removal of manganese, J. Membr. Sci., 549 (2018) 205–216.
[3] C.C. Kan, M.C. Aganon, C.M. Futalan, M.L.P. Dalida, Adsorption of Mn^{2+} from aqueous solution using Fe and Mn oxide-coated sand, J. Environ. Sci., 25 (2013) 1483–1491.
[4] J. Su, P. Bao, T. Bai, L. Deng, H. Wu, F. Liu, J. He, CotA, a multicopper oxidase from *Bacillus pumilus* WH4, exhibits manganese-oxidase activity, PLoS One, 8 (2013) e60573.
[5] A. Funes, J. De Vicente, L. Cruz-Pizarro, I.D. Vicente, The influence of pH on manganese removal by magnetic microparticles in solution, Water Res., 53 (2014) 110–122.
[6] W. Stumm, J.J. Morgan, Aquatic Chemistry: Chemical Equilibria and Rates in Natural Waters, 3rd ed., Wiley, New York, U.S.A, 1996.
[7] C. Dalai, R. Jha, V.R. Desai, Rice husk and sugarcane baggase based activated carbon for iron and manganese removal, Aquat. Procedia, 4 (2015) 1126–1133.
[8] A. Ates, G. Akgül, Modification of natural zeolite with NaOH for removal of manganese in drinking water, Powder Technol., 287 (2016) 285–291.
[9] D. Vries, C. Bertelkamp, F.S. Kegel, B. Hofs, J. Dusseldorp, J.H. Bruins, W.D. Vet, B.V.D. Akker, Iron and manganese removal: recent advances in modeling treatment efficiency by rapid sand filtration, Water Res., 10 (2017) 35–45.

[10] J.H. Bruins, B. Petrusevski, Y.M. Slokar, K. Huysman, K. Joris, J.C. Kruithof, M.D. Kennedy, Biological and physico-chemical formation of Birnessite during the ripening of manganese removal filters, Water Res., 69 (2014) 154–161.
[11] D.R. Learman, S.D. Wankel, S.M. Webb, N. Martinez, A.S. Madden, C.M. Hansel, Coupled biotic-abiotic Mn(II) oxidation pathway mediates the formation and structural evolution of biogenic Mn oxides, Geochim. Cosmochim. Acta, 75 (2011) 6048–6063.
[12] C. Li, S. Wang, X. Du, X. Cheng, M. Fu, N. H, D. Li, Immobilization of iron- and manganese-oxidizing bacteria with a biofilm-forming bacterium for the effective removal of iron and manganese from groundwater, Bioresour. Technol., 220 (2016) 76–84.
[13] W. Tang, J. Gong, L. Wu, Y. Li, M. Zhang, X. Zeng, DGGE diversity of manganese mine samples and isolation of a *Lysinibacillus* sp. efficient in removal of high Mn(II) concentrations, Chemosphere, 165 (2016) 277–283.
[14] J.H. Bruins, B. Petrusevski, Y.M. Slokar, J.C. Kruithof, M.D. Kennedy, Manganese removal from groundwater: characterization of filter media coating, Desal. Water Treat., 55 (2014) 1851–1863.
[15] Y. Cheng, T. Huang, C. Liu, S. Zhang, Effects of dissolved oxygen on the start-up of manganese oxides filter for catalytic oxidative removal of manganese from groundwater, Chem. Eng. J., 371(2019) 88–95.
[16] Y. Cheng, T.L. Huang, Y. Sun, X. Shi, Catalytic oxidation removal of ammonium from groundwater by manganese oxides filter: performance and mechanisms, Chem. Eng. J., 322 (2017) 82–89.
[17] X. Tian, R. Zhang, T.L. Huang, G. Wen, The simultaneous removal of ammonium and manganese from surface water by MeO_x: side effect of ammonium presence on manganese removal, J. Environ. Sci., 77 (2019) 346–353.
[18] Y. Cai, D. Li, Y. Liang, Y. Luo, H. Zeng, J. Zhang, Effective start-up biofiltration method for Fe, Mn, and ammonia removal and bacterial community analysis, Bioresour. Technol., 176 (2015) 149–155.
[19] C. Tizaoui, S.D. Rachmawati, N. Hilal, The removal of copper in water using manganese activated saturated and unsaturated sand filters, Chem. Eng. J., 209 (2012) 334–344.
[20] SEPA, Analytical Methods of Water and Wastewater, 4th ed., China Environmental Science Press, Beijing, China, 2002.
[21] Y.M. Guo, T.L. Huang, G. Wen, C. Xin, The simultaneous removal of ammonium and manganese from groundwater by iron-manganese co-oxide filter film: the role of chemical catalytic oxidation for ammonium removal, Chem. Eng. J., 308 (2017) 322–329.
[22] Y.M. Guo, T.L. Huang, G. Wen, C. Xin, Comparisons of the film peeling from the composite oxides of quartz sand filters using ozone, hydrogen peroxide and chlorine dioxide, J. Environ. Sci., 34 (2015) 20–27.
[23] R. Buamah, B. Petrusevski, J.C. Schippers, Oxidation of adsorbed ferrous iron: kinetics and influence of process conditions, Water Sci. Technol., 60 (2009) 2353–2363.
[24] J.R. Bargar, B.M. Tebo, U. Bergmann, S.M. Webb, P. Glatzel, Van Q. Chiu, M. Villalobos, Biotic and abiotic products of Mn(II) oxidation by spores of the marine *Bacillus* sp. strain SG-1, Am. Mineral., 90 (2005) 143–154.
[25] N.Q. Zhou, D.F. Liu, D. Min, L. Cheng, X.N. Huang, L.J. Tian, D.B. Li, H.Q. Yu, Continuous degradation of ciprofloxacin in a manganese redox cycling system driven by *Pseudomonas putida* MnB-1, Chemosphere, 211 (2018) 345–351.
[26] H. Boumaiza, A. Renard, M.R. Robinson, G. Kervern, L. Vidal, C. Ruby, L. Bergaoui, R. Coustel, A multi-technique approach for studying Na triclinic and hexagonal birnessites, J. Solid State Chem., 272 (2019) 234–243.
[27] M. Wiechen, I. Zaharieva, H. Dau, P. Kurz, Layered manganese oxides for water-oxidation: alkaline earth cations influence catalytic activity in a photosystem II-like fashion, Chem. Sci., 3 (2012) 2330–2339.
[28] P.L. Goff, N. Baffier, S. Bach, J.P. Pereira-Ramos, Synthesis, ion exchange and electrochemical properties of lamellar phyllomanganates of the birnessite group, Mater. Res. Bull., 31 (1996) 63–75.
[29] A. Naidja, C. Liu, P. M. Huang, Formation of protein-birnessite complex: XRD, FTIR, and AFM analysis, J. Colloid Interface Sci., 251 (2002) 46–56.
[30] Q. Wang, P. Yang, M. Zhu, Effects of metal cations on coupled birnessite structural transformation and natural organic matter adsorption and oxidation, Geochim. Cosmochim. Acta, 250 (2019) 292–310.
[31] C. Julien, M. Massot, R. Baddour-Hadjean, S. Franger, S. Bach, J.P. Pereira-Ramos, Raman spectra of birnessite manganese dioxides, Solid State Ionics, 159 (2003) 345–356.
[32] J.E. Post, Manganese oxide minerals: crystal structures and economic and environmental significance, Proc. Natl. Acad. Sci. U.S.A., 96 (1999) 3447–3454.
[33] S. Luo, L. Duan, B. Sun, M. Wei, X. Li, A. Xu, Manganese oxide octahedral molecular sieve (OMS-2) as an effective catalyst for degradation of organic dyes in aqueous solutions in the presence of peroxymonosulfate, Appl. Catal., B, 164 (2015) 92–99.
[34] J.M. Cerrato,W.R. Knocke, M.F. Hochella, Jr., A.M. Dietrich, A. Jones, T.F. Cromer, Application of XPS and solution chemistry analysis to investigate soluble manganese removal by MnOx(s)-coated media, Environ. Sci. Technol., 45 (2011) 10068–10074.
[35] V.P. Santos, M.F.R. Pereira, J.J.M. Órfão, J.L. Figueiredo, The role of lattice oxygen on the activity of manganese oxides towards the oxidation of volatile organic compounds, Appl. Catal., B, 99 (2010) 353–363.
[36] N.H. Wang, S.L. Lo, Preparation, characterization and adsorption performance of cetyltrimethylammonium modified birnessite, Appl. Surf. Sci., 299 (2014) 123–130.
[37] H.W. Nesbitt, D. Banerjee, Interpretation of XPS Mn(2p) spectra of Mn oxyhydroxides and constraints on the mechanism of MnO_2 precipitation, Am. Mineral., 83 (1998) 305–315.
[38] J.H. Park, B.S. Kim, C.M. Chon, Characterization of iron and manganese minerals and their associated microbiota in different mine sites to reveal the potential interactions of microbiota with mineral formation, Chemosphere, 191 (2018) 245–252.
[39] X.Z. Lin, A.G. Gao, H.W. Chen, Isolation and phylogenetic analysis of cultivable manganese bacteria in sediments from the Arctic ocean, Acta Ecol. Sin., 28 (2008) 6364–6370.
[40] V.R. Cahyani, J. Murase, E. Ishibashi, S. Asakawa, M. Kimura, Bacterial communities in manganese nodules in rice field subsoils: estimation using PCR-DGGE and sequencing analysis, Soil Sci. Plant Nutr., 53 (2007) 575–84.
[41] C.R. Anderson, H.A. Johnson, N. Caputo, R.E. Davis, J.W. Torpey, B.M. Tebo, Mn(II) oxidation is catalyzed by heme peroxidases in "*Aurantimonas manganoxydans*" Strain SI85–9A1 and *Erythrobacter* sp. Strain SD-21, Appl. Environ. Microbiol., 75 (2009) 4130–4138.
[42] G.J. Dick, Y.E. Lee, B.M. Tebo, Manganese(II)-oxidizing *Bacillus* spores in Guaymas Basin hydrothermal sediments and plumes, Appl. Environ. Microbiol., 72 (2006) 3184–3190.
[43] C.A. Francis, K.L. Casciotti, B.M. Tebo, Localization of Mn(II)-oxidizing activity and the putative multicopper oxidase, MnxG, to the exosporium of the marine *Bacillus* sp. strain SG-1, Arch. Microbiol., 178 (2002) 450–456.
[44] K.H. Nealson, J. Ford, Surface enhancement of bacterial manganese oxidation: implications for aquatic environments, Geomicrobiol. J., 2 (1980) 21–37.
[45] R.A. Rosson, K.H. Nealson, Manganese binding and oxidation by spores of a marine *Bacillus*, J. Bacteriol., 151 (1982) 1027–1034.
[46] K. Toyoda, B.M. Tebo, Kinetics of Mn(II) oxidation by spores of the marine *Bacillus* sp. SG-1, J. Bacteriol., 189 (2016) 58–69.
[47] L.G. Waasbergen, J.A. Hoch, B.M. Tebo, Genetic analysis of the marine manganese-oxidizing *Bacillus* sp. strainSG-1: protoplast transformation, Tn917 mutagenesis, and identification of chromosomal loci involved in manganese oxidation, J. Bacteriol., 175 (1993) 7594–7603.
[48] X. Zeng, M. Zhang, Y. Liu, W. Tang, Manganese(II) oxidation by the multi-copper oxidase CopA from *Brevibacillus panacihumi* MK-8, Enzyme Microb. Technol., 117 (2018) 79–83.

[49] E. Gregory, J.T. Staley, Widespread distribution of ability to oxidize manganese among freshwater bacteria, Appl. Environ. Microbiol., 44 (1982) 509–511.
[50] P. Mouchet, From conventional to biological removal of Fe and Mn in France, J. Am. Water Works Assn., 84 (1992) 158–166.
[51] C.A. Francis, E.-M. Co, B.M. Tebo, Enzymatic manganese(II) oxidation by a marine *alpha-Proteobacterium*, Appl. Environ. Microbiol., 67 (2001) 4024–4029.
[52] M.J. Carmichael, S.K. Carmichael, C.M. Santelli, A. Strom, S.L. Bräuer, Mn(II)-oxidizing bacteria are abundant and environmentally relevant members of ferromanganese deposits in caves of the Upper Tennessee River Basin, Geomicrobiol. J., 30 (2013) 779–800.
[53] L.F. Adams, W.C. Ghiorse, Characterization of extracellular Mn^{2+}-oxidizing activity and isolation of an Mn^{2+}-oxidizing protein from *Leptothrix discophora* SS-1, J. Bacteriol., 169 (1987) 1279–1285.
[54] P.L.A.M. Corstjens, J.P.M. De Vrind, P. Westbroek, E.W. De V.-De Jong, Enzymatic iron oxidation by *Leptothrix discophora*: identification of an iron-oxidizing protein, Appl. Environ. Microbiol., 58 (1992) 450–454.
[55] I.A.E. Gheriany, D. Bocioaga, A.G. Hay, W.C. Ghiorse, M.L. Shuler, L.W. Lion, Iron requirement for Mn(II) oxidation by *Leptothrix discophora* SS-1, Appl. Environ. Microbiol., 75 (2009) 1229–1235.
[56] Y.M. Nelson, L.W. Lion, W.C. Ghiorse, M.L. Shuler, Production of biogenic Mn oxides by *Leptothrix discophora* SS-1 in a chemically defined growth medium and evaluation of their Pb adsorption characteristics, Appl. Environ. Microbiol., 65 (1999) 175–180.
[57] J.P. Ridge, M. Lin, E.I. Larsen, M. Fegan, A.G. McEwan, L.I. Sly, A multicopper oxidase is essential for manganese oxidation and laccase-like activity in *Pedomicrobium* sp. ACM 3067, Environ. Microbiol., 9 (2007) 944–953.
[58] G.-J. Brouwers, J.P.M. De Vrind, P.L.A.M. Corstjens, P. Cornelis, C. Baysse, E.W. De V.-De Jong, cumA, a gene encoding a multicopper oxidase, is involved in Mn^{2+} oxidation in *Pseudomonas putida* GB-1, Appl. Environ. Microbiol., 65 (1999) 1762–1768.
[59] R. Caspi, B.M. Tebo, M.G. Haygood, c-Type cytochromes and manganese oxidation in *Pseudomonas putida* MnB1, Appl. Environ. Microbiol., 64 (1998) 3549–3555.
[60] S.J. Parikh, J. Chorover, FTIR spectroscopic study of biogenic Mn-oxide formation by *Pseudomonas putida* GB-1, Geomicrobiol. J., 22 (2005) 207–218.
[61] S. Jiang, D.G. Kim, J. Kim, S.O. Ko, Characterization of the biogenic manganese oxides produced by *Pseudomonas putida* strain MnB1, Environ. Eng. Res., 15 (2011) 183–190.

Supplementary information

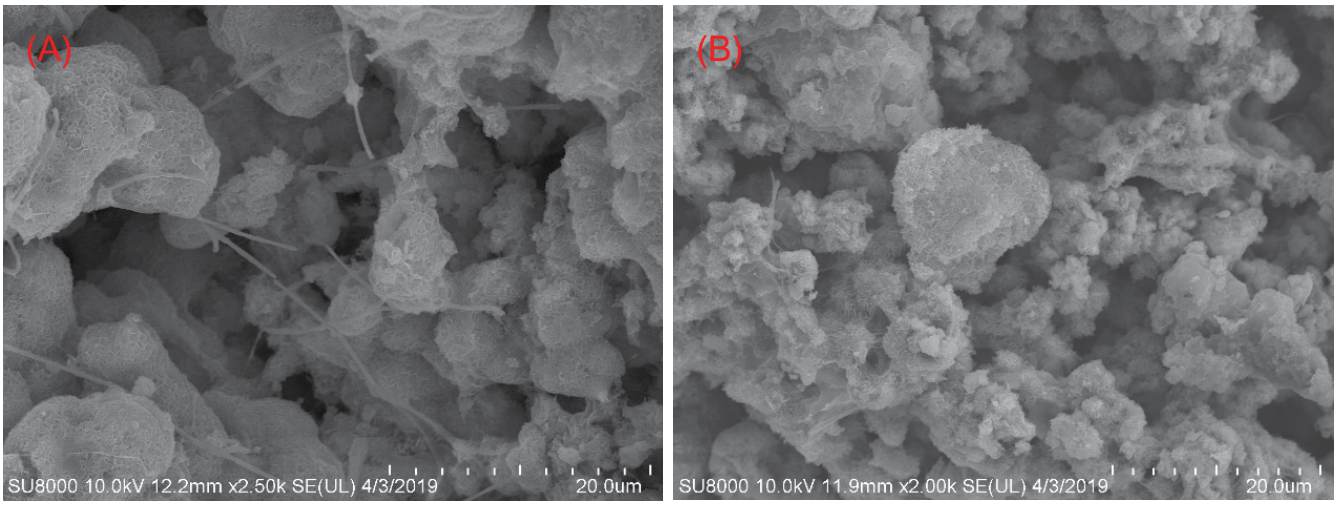

Fig. S1. SEM images of the surface of manganese sand (a) unsterilized and (b) sterilized with a bar of 20 μm.

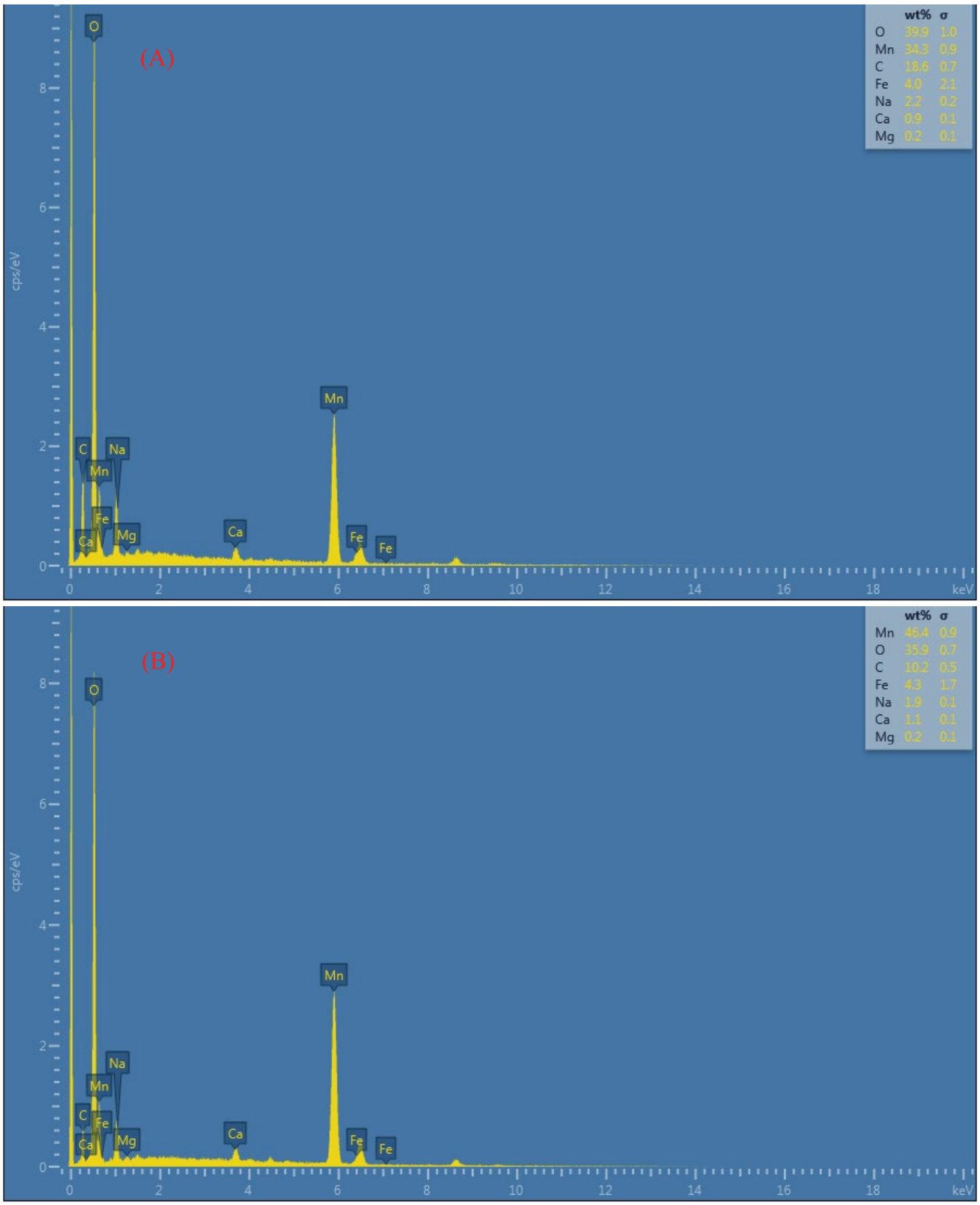

Fig. S2. Composition elements of manganese oxides formed on the (a) *R*1 and (b) *R*2.

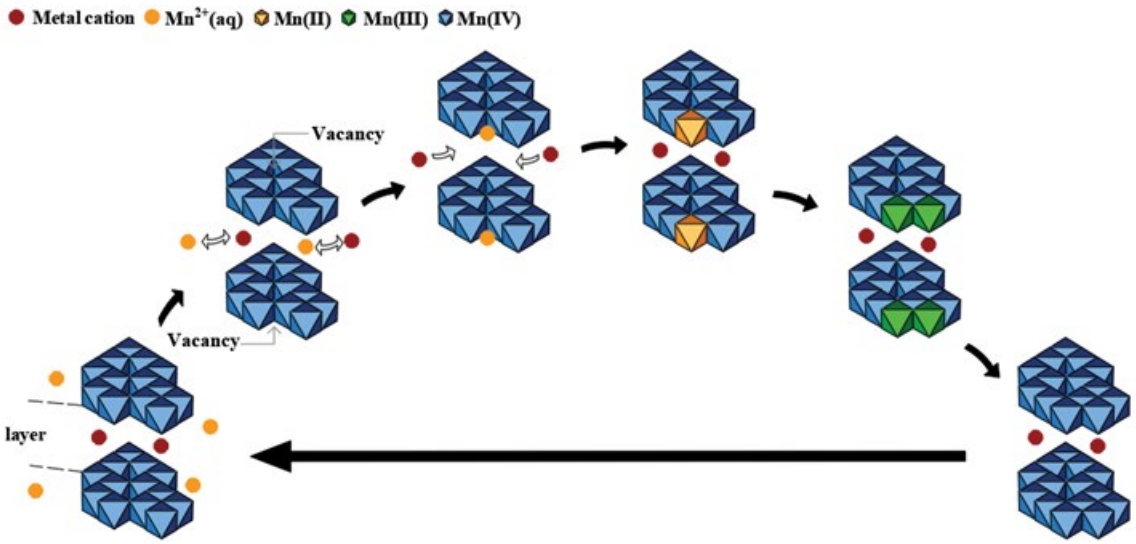

Fig. S3. Reaction pathway of a cyclic autocatalytic process for manganese removal by Birnessite.

Table S1
OTUs, diversity and richness indices of the microbial samples from *R*1 and *R*2

	Similarity 0.97			
Samples	OTUs	Shannon	Simpson	Coverage (%)
*R*1	1,474	4.22	0.04	99.34
*R*2	1,737	4.68	0.02	99.27